Appl. Phys. B (2016) 122:135
DOI 10.1007/s00340-016-6417-9

Applied Physics B
Lasers and Optics

Thermal lensing in Nd:YVO_4 laser with in-band pumping at 914 nm

Tanant Waritanant[1] · **Arkady Major**[1]

Received: 4 November 2015 / Accepted: 13 April 2016 / Published online: 2 May 2016

Abstract Thermal lensing in an Nd:YVO_4 laser system operating at 1064 nm with in-band pumping at 914 nm was characterized. The focal length of the thermal lens in the crystal was calculated using ABCD matrix formalism from the experimental data of the output beam diameter measurements made at different output power levels. The determined focal lengths of thermal lens were as strong as 4.4 diopters at 3.5 W of output power. The experimental results agree well with the finite element analysis of the developed laser system. A numerical comparison of the thermal lensing effect with 914-, 888-, 880-nm pumping, and with a standard 808-nm pumping was also made, demonstrating effective reduction of thermal lensing up to 2.1 times.

1 Introduction

Nd:vanadate (Nd:YVO_4) laser crystal has been extensively studied as an alternative to Nd:YAG for medium-range power applications due to several advantages such as its high emission cross section, broader absorption profile, and natural birefringence [1, 2]. However, at high output power, the Nd:YVO_4 laser is limited by the inferior thermal properties which lead to a stronger thermal gradient [3–8]. The induced thermal gradient degrades the optical properties of the gain medium and reduces the stability of a laser cavity through thermal lensing effect which in turn lowers the output beam quality and the optical efficiency. Ultimately, large thermal gradient can result in failure of the material. To overcome this limitation, recent studies have focused on diode pumping of Nd:YVO_4 lasers at other absorption lines with longer wavelengths such as 880, 888, and 914 nm to produce 1064-nm laser output [9–15]. This results in the reduction in quantum defect.

The smaller quantum defect from the longer pump wavelengths translates directly to a smaller amount of heat generated within the crystal in continuous wave regime due to the relaxation process with minimal effect from energy transfer upconversion (ETU) and quenching [16]. By using 914 nm as the pump wavelength instead of the conventional 808 nm, the quantum defect is reduced from 24.1 to 14.1 %. The reduction in quantum defect directly affects the thermal lensing effect inside the laser crystal which is created by three mechanisms: change in refractive index profile due to thermo-optic effect (dn/dT), change in refractive index profile due to mechanical stress, and surface bulging of the laser crystal. The quantification of the thermal lensing effect caused by the different values of quantum defect will benefit the power scaling design of Nd:YVO_4 lasers.

There is, however, no report focusing on thermal lensing in Nd:YVO_4 lasers with low quantum defect pumping at 914 nm. Moreover, there are also no reports on comparative studies of this effect with different values of quantum defect. This paper addresses these issues and presents a comprehensive study of thermal lensing effect in 914-nm diode-pumped Nd:YVO_4 laser. The work combined experimental data with finite element analysis of the developed laser system and showed good agreement. Using finite element analysis, a numerical comparison of the thermal lensing effect with 914-, 888-, 880-nm pumping, and with a standard 808-nm pumping was also made, demonstrating effective reduction of thermal lensing up to 2.1 times.

✉ Arkady Major
a.major@umanitoba.ca

[1] Department of Electrical and Computer Engineering, University of Manitoba, Winnipeg, Canada

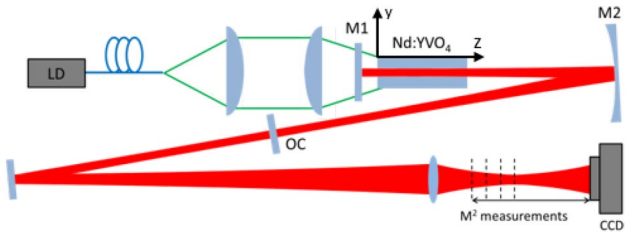

Fig. 1 Schematic diagram of the Nd:YVO_4 laser used in the thermal lensing experiment

2 Experimental details

The laser cavity used in the thermal lens measurement is shown in Fig. 1. The experiment utilized a 3-mirror laser cavity arrangement with a 0.5 at.% doped a-cut $3 \times 3 \times 12$ mm^3 Nd:YVO_4 crystal as the gain medium (Castech) and a 10 % output coupler. The first laser reflector is a dichroic mirror placed 20 mm in front of the gain medium allowing the pump laser at 914 nm into the cavity. Both surfaces of Nd:YVO_4 crystal were anti-reflection coated at 914 and 1064 nm. The Nd:YVO_4 crystal was water-cooled at 16 °C on the top and bottom surfaces using metal blocks. The system was pumped by a randomly polarized fiber-coupled 914-nm diode laser with NA of 0.12. The pump laser was focused to the center of the gain medium with a spot size radius of 275 μm.

The cavity was designed such that the laser mode size was 275 μm at the center of the crystal and fully overlapped with the pump beam at the highest output power while the laser mode size at the output coupler was allowed to change freely. The pump-mode overlap efficiency changed by less than 5 % for all thermal lens values to ensure good mode matching. This resulted in higher sensitivity of the laser output profile to thermal lensing. A beam profiler was used to monitor the changes in the laser beam size.

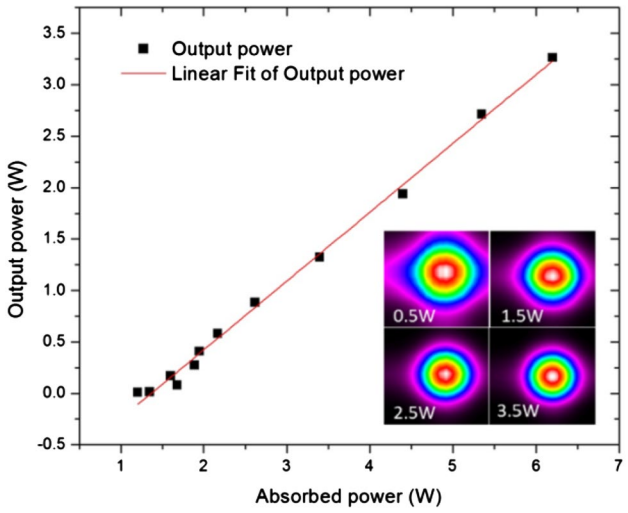

Fig. 2 Laser output power versus absorbed pump power and output laser beam profiles at different output power levels

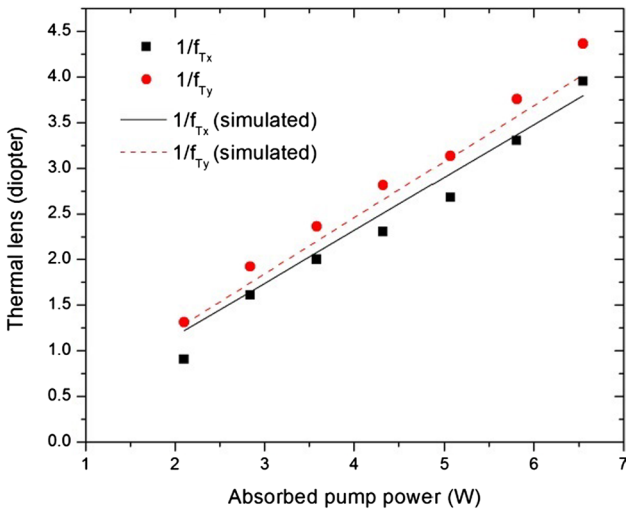

Fig. 3 Calculated thermal lens power from the experiment (*dots*) and FEA analysis simulation results (*lines*) for horizontal and vertical directions

3 Results and discussions

Figure 2 shows the experimental results for the laser output power versus the absorbed pump power. The slope efficiency was 66.9 %. The laser system produced the highest output power of 3.52 W with 56.8 % of optical-to-optical efficiency with respect to the absorbed pump power. The beam quality factor was approximately 1.4 throughout the experiment. The measured absorption coefficient was 0.23 cm^{-1} which is comparable to other reports [13]. The absorbed power was 24 % of the incident pump power. Due to the low absorption coefficient of Nd:YVO_4 at 914 nm compared to other traditional absorption lines, longer crystal, higher doping level, higher crystal temperature, or multiple-pass pumping schemes can be utilized in order to increase the absorbed pump power further.

The laser output beam profiles at different output power levels are also shown in the inset in Fig. 2. Changes in the output beam profile as the output power level changes clearly show the effect of thermal lensing inside the laser cavity.

The laser beam size and divergence were monitored outside the cavity as the pump power was increased. At each output power level, the dioptric power of the effective

thermal lens (assumed to be located at the pump beam waist in the laser crystal) was determined by comparing the experimental data with the ABCD matrix simulations that took into account the measured beam quality factor (M^2). In each case, the simulated output beam size and divergence were matched with the experimental results with thermal lens value being a free parameter [17].

The resulting thermal lens dioptric powers for all power levels are shown in Fig. 3. The maximum values are 3.95 m^{-1} horizontally (x) and 4.37 m^{-1} vertically (y) at 6.55 W. Thermal lensing was stronger in the vertical direction because of the larger difference in temperature gradient due to the direction of cooling. Compared to the previous records of thermal lensing in an a-cut Nd:YVO_4 crystal pumped at 808 [18–20], pumping at 914 nm creates a weaker thermal lens at the same level of the absorbed pump power.

To verify the accuracy of the measurements, finite element analysis (FEA) of thermal lensing under the same pumping geometry was done using the commercially available LASCAD software package and the most recent report of temperature coefficient of refractive index (dn/dt) [21]. The pump beam divergence, thermo-optic effect, and surface deformation were taken into account in the simulation. The pump beam divergence was 23 mrad. The dioptric powers of thermal lens obtained from the experimental data are compared to the FEA simulation results in Fig. 3. As can be seen, the simulated thermal lens dioptric power is in good agreement with experimental data.

Using the developed model for further studies, FEA was also done for 888-, 880-, and 808-nm pumping under the same conditions (absorbed pump power level, pump spot size, and pump divergence) as in 914-nm pumping case.

The differences between pumping at different wavelengths were quantum defect and absorption coefficient (α) at pump wavelength. The absorption coefficients of 0.5 % doped a-cut Nd:YVO_4 crystal used in the FEA simulations were 0.23, 0.73, 5.3, and 7.0 cm^{-1}, and the quantum defects were 14.1, 16.5, 17.2, and 24.1 % for 914-, 888-, 880-, and 808-nm pumping schemes, respectively. The absorption coefficients used above were previously reported values [4, 5, 9, 13]. The absorption coefficient for 808-nm pumping was much lower than the peak absorption of the 0.5 % doped Nd:YVO_4 crystal due to the unpolarized pumping condition and the difference in bandwidth of the absorption band of Nd:YVO_4 and the spectrum of the pump (3 nm) which was measured by Xiong et al. [5]. In general, a higher value of the pump absorption coefficient would result in stronger thermal lensing. The simulated results are compared in Fig. 4 showing the highest thermal lens dioptric power for 808-nm pumping as expected.

Using the laser crystal thermal lens sensitivity factor (M) as defined as $M = \mathrm{d}(1/f)/\mathrm{d}P_{\mathrm{abs}}$ which describes how much

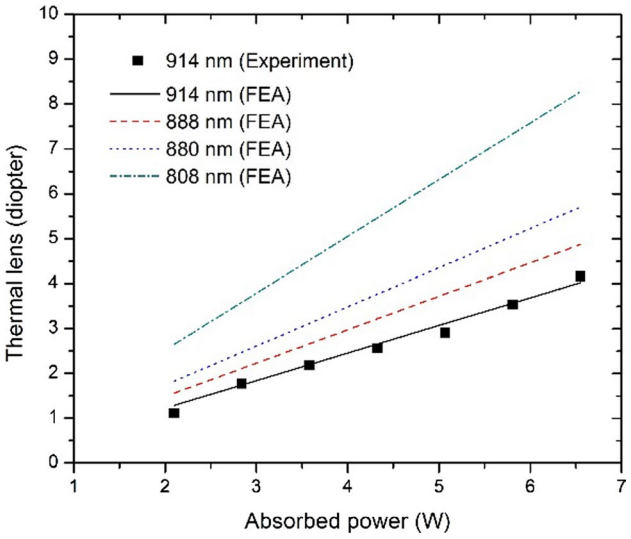

Fig. 4 Thermal lens dioptric powers simulated from FEA with four different pumping schemes and experimentally obtained from 914-nm pumping

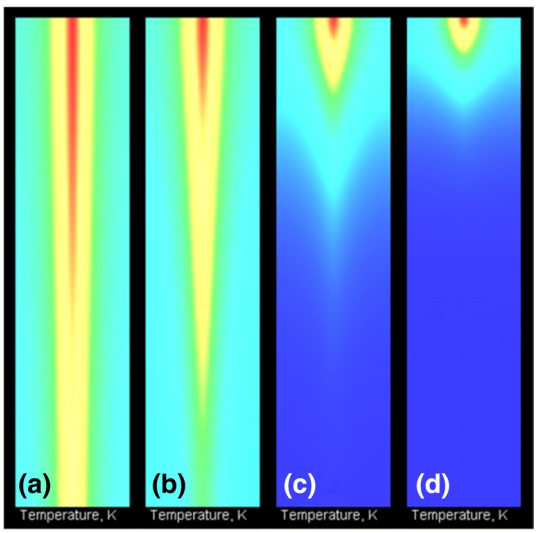

Fig. 5 Temperature distribution plots from FEA simulations for 0.5 at.% Nd:YVO_4 pumped with **a** 914, **b** 888, **c** 880, and **d** 808 nm at the same level of absorbed pump power (6.55 W). The highest temperatures at the input facets were 295.9, 299.7, 327.1, 348.3 °C, respectively

the optical power of the induced lens changes due to the absorbed pump power, the results above show that thermal lens power with 914-nm pumping is reduced by a factor of 2.1 from the 808-nm pumping.

To get a better understanding of the physical conditions accompanying thermal lens formation, temperature distribution plots inside the gain medium under different pump wavelengths from FEA simulations at 6.55 W of absorbed pump power are shown in Fig. 5. Due to the low pump

absorption coefficient at 914 nm, the heat load is spread in a larger volume, thus minimizing stress and temperature rise. This reduction in mechanical stress and temperature gradient changes the geometry of the thermal lens and ultimately reduces its dioptric power.

Therefore, reduction of thermal lensing can be explained by two reasons, first, the reduction in quantum defect and secondly, the shape of the thermal lens geometry. Another parameter that can also affect thermal lens dioptric power is the pump spot size, since thermal lens dioptric power is inversely proportional to its area [1]. Therefore, thermal lens to some extent can be controlled by the selection of a larger pump spot size albeit at the expense of the increased threshold pump power and thus lower output power.

4 Conclusion

Thermal lensing effect in a 914-nm diode-pumped Nd:YVO_4 laser has been studied in order to assess its strength. FEA simulation was also done to compare the thermal lensing effect with 914-, 888-, 880-, and 808-nm pumping wavelengths. The results show that the thermal lens power was significantly reduced because of the difference in quantum defect and the thermal lens geometry. Our results indicate that in-band pumping at 914 nm offers significant advantages for development of high average power Nd:YVO_4 and other Nd-ion laser oscillators in continuous wave regime.

Acknowledgments The authors would like to acknowledge funding of this project provided by the Natural Sciences and Engineering Research Council of Canada, Western Economic Diversification Canada, and the University of Manitoba.

References

1. W. Koechner, *Solid-State Laser Engineering* (Springer, Berlin, 1999)
2. G. Turri, H.P. Jenssen, F. Cornacchia, M. Tonelli, M. Bass, J. Opt. Soc. Am. B **26**, 2084 (2009)
3. A. Sennaroglu, Appl. Opt. **38**, 3253 (1999)
4. F. Song, C. Zhang, X. Ding, J. Xu, G. Zhang, Appl. Phys. Lett. **81**, 2145 (2002)
5. Z. Xiong, Z.G. Li, N. Moore, W.L. Huang, G.C. Lim, IEEE J. Quantum Electron. **39**, 979 (2003)
6. X. Huai, Z. Li, Appl. Phys. Lett. **92**, 041121 (2008)
7. R. Soulard, A. Zinoviev, J.L. Doualan, E. Ivakin, O. Antipov, R. Moncorge, Opt. Express **18**, 1553 (2010)
8. Y.R. Peng, Y. Xin, C.D. Ying, C. Fei, L.X. Dong, M.Y. Fei, Y.J. Hua, Chin. Phys. B **21**, 024208 (2012)
9. L. McDonagh, R. Wallenstein, R. Knappe, A. Nebel, Opt. Lett. **31**, 3297 (2006)
10. L. McDonagh, R. Wallenstein, A. Nebel, Opt. Lett. **32**, 1259 (2007)
11. N. Pavel, C. Krankel, R. Peters, K. Petermann, G. Huber, Appl. Phys. B **91**, 415 (2008)
12. Y.J. Wang, W.H. Yang, H.J. Zhou, M.R. Huo, Y.H. Zheng, Opt. Express **21**, 18068 (2013)
13. D. Sangla, M. Castaing, F. Balembois, P. Georges, Opt. Lett. **34**, 2159 (2009)
14. X. Yu, F. Chen, R. Yan, X. Li, J. Yu, Z. Zhang, Chin. Opt. Lett. **8**, 499 (2010)
15. X. Ding, S.J. Yin, C.P. Shi, X. Li, B. Li, Q. Sheng, X.Y. Yu, W.Q. Wen, J.Q. Yao, Opt. Express **19**, 14315 (2011)
16. X. Delen, F. Balembois, O. Musset, P. Georges, J. Opt. Soc. Am. B **28**, 52 (2011)
17. H. Mirzaeian, S. Manjooran, A. Major, SPIE Proc. **9288**, 928802-1 (2014)
18. I.O. Musgrave, W.A. Clarkson, D.C. Hanna, in *Conference on Lasers and Electro-Optics* (Optical Society of America, 2001), pp. 171–172
19. L. McDonagh, R. Wallenstein, in *Conference on Lasers and Electro-Optics* (Optical Society of America, 2005), p. CMS5
20. T. Li, Z. Zhuo, X. Li, H. Yang, Y. Zhang, Chin. Opt. Lett. **5**, 175 (2007)
21. Y. Sato, T. Taira, Opt. Mater. Express **4**, 876–888 (2014)